Published by :
http://www.ijert.org

International Journal of Engineering Research & Technology (IJERT)
ISSN: 2278-0181
Vol. 10 Issue 04, April-2021

Design, Analysis, and Fabrication of an Electric Dune Buggy

Prateek Mahapatra
Department of Mechanical Engineering
Manav Rachna University
Faridabad, India

Shivam Kumar Singh
Department of Mechanical Engineering
Manav Rachna University
Faridabad, India

Ritvik Manocha
Department of Mechanical Engineering
Manav Rachna University
Faridabad, India

Manan Aggarwal
Department of Mechanical Engineering
Manav Rachna University
Faridabad, India

Abstract **- The main objective of this paper is to cover all the aspects of designing an electric dune buggy. A new and lighter dune buggy chassis is proposed in this study. A CAD model of the chassis was made using Autodesk Fusion 360 and its Finite Element Analysis was done on the same. 4g, 6g, 8g, 10g, and 16g loading criterion was used to simulate the impact behavior on the chassis. The design and development comprised of material selection, chassis design, cross-section determination, determining strength requirements of the roll cage. We followed Ackermann's steering geometry to set up our steering. We used Lotus Shark for designing and testing the suspension system of the dune buggy. A suitable motor was selected by determining the required motor power rating, torque, and r.p.m for our design. We selected the battery in consideration of the motor. Most of the components used have been chosen as per the ease of availability and reliability. We selected the brake in accordance with the top speed of the vehicle and the clamping force required.**

The results of simulations done in Autodesk Fusion 360 which was performed under different loading conditions showed that this design has demonstrated adequate resistance against deformation in front, back, and side-impact tests. In every situation, the factor of safety was more than one. Therefore, it can be inferred that the proposed design was completely safe under testing conditions. However, detailed modeling and simulation studies are needed before testing it in real-life conditions. The results of the simulations generated by the Lotus Shark showed that the suspension geometry selected for our design has minimal bump steer, change in camber angle, and change in toe angle during suspension bump and droop. A dune buggy is a vehicle designed for use on dunes and roads. Such a type of vehicle is primarily used for recreational purposes.

Keywords – Analysis; Dune Buggy; Electric Vehicle.

I . INTRODUCTION

A dune buggy is also known as a beach buggy is a recreational motor vehicle with large wheels, and wide tires, designed for use on dunes, beaches, roads, or deserts. An engine or electric motor is used to drive the vehicle, which can be powered by fuel or electricity, respectively. In our design, the zero-emission drive of the dune buggy is made up of the electric motor integrated into the rear axle together with the power electronics. The concept car is a single-seater; however, some recreational models may accommodate an additional seat for a passenger. In addition to suitable driving capability, it is essential to use a strong chassis in a dune buggy capable of providing complete protection to the driver. The average weight of an outdoor dune buggy is 600-800 kg.

II. CHASSIS

A. Experimental Procedure

The electric dune buggy is designed in Autodesk Fusion 360 software. This design attempts to optimize in terms of durability, weight, and performance. In this proposed structure, rigid tubular sections of aluminum (Al-6061) have been used in our design. The chemical composition and mechanical and physical properties of Aluminum (Al-6061) are shown in Tables I. and II., respectively. This material is used to withstand extreme stress during driving conditions. All the components of this electric dune buggy chassis were enclosed efficiently to ensure driver safety at the time of impact. The chassis frame is a fundamental and supporting part of the entire vehicle. The chassis must be sufficiently stable so that it can efficiently absorb the vibrations generated when the buggy is moving. The use of Aluminum (Al-6061) tubular constructions in this design may be able to meet these requirements. Also, the stability of the chassis is ensured when all its main parts are solidly interconnected. This is not an articulation but a significant need for solid construction. However, articulated connections are only permitted for the support of the steering knuckle and steering column.

TABLE I. Chemical composition of Aluminum Al-6061

Elements	Al	Mg	Si	Cu	Cr
Wt.%	97.9	1	0.60	0.28	0.20

International Journal of Engineering Research & Technology (IJERT)
ISSN: 2278-0181
Vol. 10 Issue 04, April-2021

TABLE II. Mechanical & physical properties of Aluminum Al-6061

S. No.	Property	Value
1.	Density	2.7 g/cm^3
2.	Young Modulus	69 GPa
3.	Poisson's Ratio	0.33
4.	Ultimate Tensile Strength	310 MPa
5.	Yield Strength	275 MPa

B. Design Considerations & Testing

The center of gravity of the chassis was determined by Autodesk Fusion 360. The top priority of this design was to keep the frame of the chassis as light as possible. The weight of the vehicle is a major factor in vehicle performance when the power of the vehicle is limited. The chassis frame is one of the heaviest components of the car. Owing to that factor, special attention is being paid to reduce the weight of the vehicle frame. To reduce the overall weight, it is very important to determine the proper design of the chassis and to employ the right materials at the appropriate locations. The use of Finite Element Analysis (FEA) can provide overall support to meet baseline safety design requirements for the car chassis. The use of FEA can make the chassis design process efficient and effective, and helps detect high or low-stress situations in different members at testing conditions. In this study, Aluminum (Al-6061) pipes with a wall thickness of 10.16 mm and an outer diameter of 50.48 mm have been used to make the chassis frame. This material has been chosen due to its weight reduction capability and beneficial properties. The overall weight of the chassis can be reduced considerably by taking into account certain facts such as the selection of suitable material, simpler design, the use of fewer members, etc. The weight of the chassis designed for this study was 53.337 kg and the gross weight of the vehicle with the driver is estimated to be 397.8 kg. In this investigation, structural analysis such as static and impact analysis was performed using FEA. Also, the behavior of the designed chassis was reviewed under various conditions. Thus, the severity of any undesirable outcome was estimated and an attempt was made to examine the need for any necessary modifications to the design.

C. Study of Chassis at Different Loading Conditions

In this section, this design of dune buggy was made from Aluminum Al-6061 and was tested at different load conditions. The results for the front, rear and side impact test are compiled in Table III., IV., and V. respectively.

FRONT IMPACT TEST FOR 16g LOAD

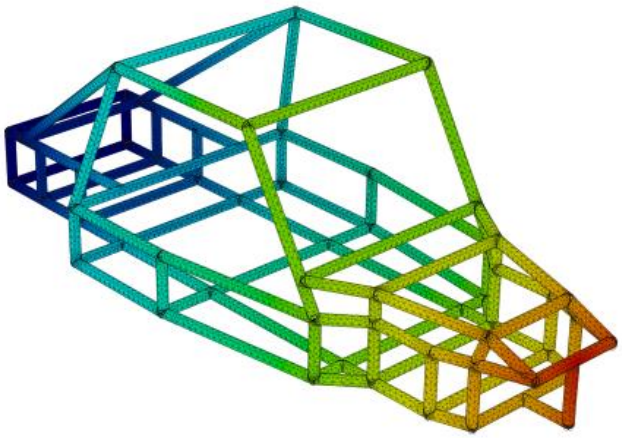

A. Front Deformation

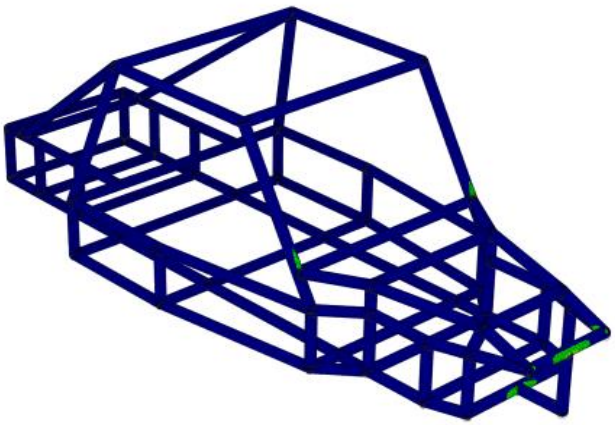

B. Front Safety Factor

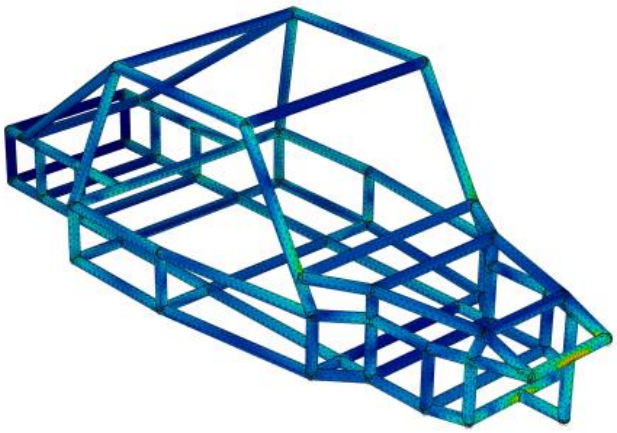

C. Front Stress

International Journal of Engineering Research & Technology (IJERT)
ISSN: 2278-0181
Vol. 10 Issue 04, April-2021

REAR IMPACT TEST FOR 16g LOAD

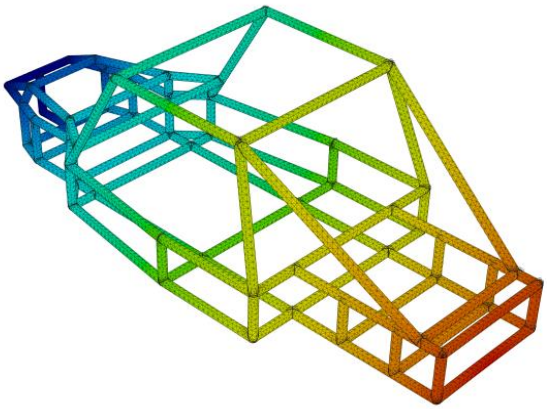

A. Rear Deformation

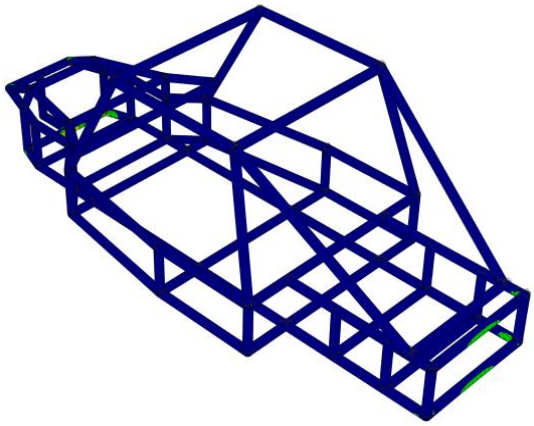

B. Rear Safety Factor

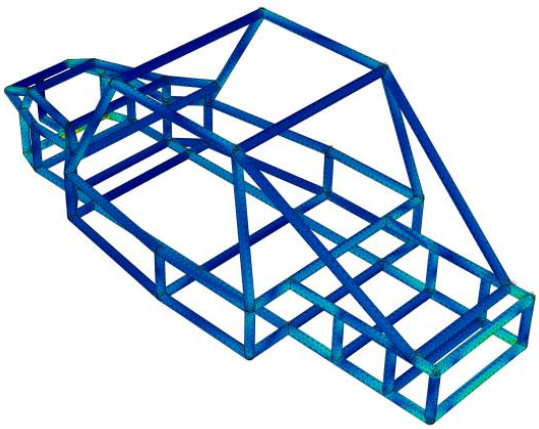

C. Rear Stress

SIDE IMPACT TEST FOR 6g LOAD

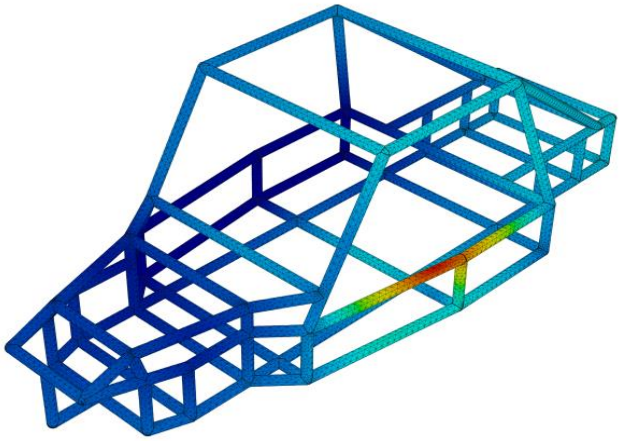

A. Side Deformation

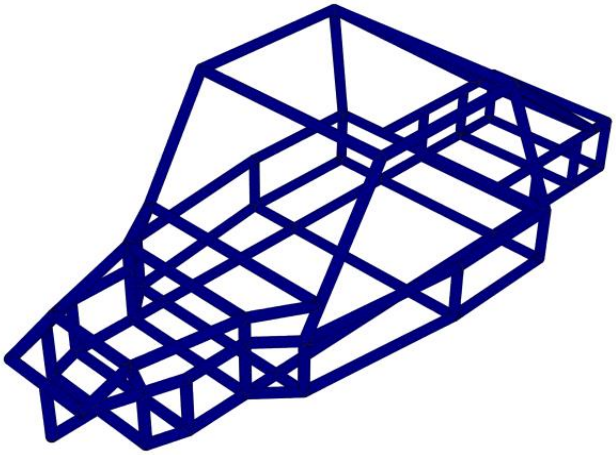

B. Side Safety Factor

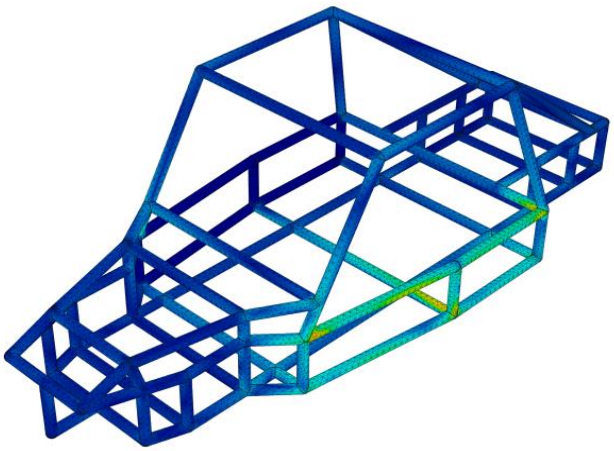

C. Side Stress

International Journal of Engineering Research & Technology (IJERT)
ISSN: 2278-0181
Vol. 10 Issue 04, April-2021

TABLE III. Front Impact Test

Material	Al-6061				
Load Consideration	4g	6g	8g	10 g	16 g
Applied Force (KN)	5.507	8.262	11.014	13.767	22.028
Min Strain	6.292E-11	6.3E-11	6.308E-11	6.317E-11	6.333E-11
Max Strain	5.723E-04	8.593E-04	0.001146	0.001433	0.002293
Von-misses Stress (MPa) Min.	3.34E-06	3.346E-06	3.355E-06	3.341E-06	3.318E-06
Von-misses Stress (MPa) Max.	27.24	40.87	54.48	68.1	109
Deformation (mm)	0.5478	1.644	2.825	4.018	7.612
Min Safety Factor	10.1	6.729	5.048	4.038	2.524
Max Safety Factor	15	15	15	15	15
Design Consideration	SAFE	SAFE	SAFE	SAFE	SAFE

TABLE IV. Rear Impact Test

Material	Al-6061				
Load Consideration	4g	6g	8g	10 g	16 g
Applied Force (KN)	5.507	8.262	11.014	13.767	22.028
Min Strain	5.24E-11	5.333E-11	5.466E-11	5.637E-11	5.719E-11
Max Strain	0.001324	0.001688	0.002052	0.002416	0.03508
Von-misses Stress (MPa) Min.	3.18E-06	3.246E-06	3.31E-06	3.397E-06	3.949E-06
Von-misses Stress (MPa) Max.	57.41	72.89	88.36	103.8	150.3
Deformation (mm)	5.953	7.1	8.249	9.401	12.86
Min Safety Factor	6.87	4.581	3.436	2.749	1.718
Max Safety Factor	15	15	15	15	15
Design Consideration	SAFE	SAFE	SAFE	SAFE	SAFE

TABLE V. Side Impact Test

Material	Al-6061	
Load Consideration	4g	6g
Applied Force (KN)	5.507	8.262
Min Strain	4.494E-11	4.494E-11
Max Strain	5.336E-04	8.125E-04
Von-misses Stress (MPa) Min.	2.525E-06	2.996E-06
Von-misses Stress (MPa) Max.	29.61	43.83
Deformation (mm)	0.9992	1.534
Min Safety Factor	9.286	6.275
Max Safety Factor	15	15
Design Consideration	SAFE	SAFE

These results indicate that the material used in the current investigation not only meets the requirements for our design but also showed sufficient resistance against front, rear and side-impact tests.

III. SUSPENSION

The overall purpose of a suspension system is to absorb impacts from coarse irregularities such as bumps and distribute that force with the least amount of discomfort to the driver. A camber of 2° and a caster of 10° was set for the front wheels. The shock absorbers and spring coefficients were set to provide a smooth and well-performing ride. The suspension not only dictates the path of the relative motion but also controls forces transmitted by sprung and un-sprung mass. The Double-A wishbone suspension system was selected for its simple design and ability to provide good travel. We used Lotus Shark suspension analysis software to analyze and simulate the suspension system selected for our design.

International Journal of Engineering Research & Technology (IJERT)
ISSN: 2278-0181
Vol. 10 Issue 04, April-2021

TABLE VI. Suspension Hardpoints

Points	X (mm)	Y (mm)	Z (mm)
Lower wishbone front pivot	-375.9550	-296.7990	30.6930
Lower wishbone rear pivot	-134.6550	-296.7990	30.6930
Lower wishbone outer ball joint	-270.7660	-626.4660	-48.2280
Upper wishbone front pivot	-375.9550	-296.7990	185.1750
Upper wishbone rear pivot	-134.6550	-296.7990	185.1750
Upper wishbone outer ball joint	-239.8440	-615.0610	126.4910
Damper wishbone end	-270.7390	-553.4880	-47.7240
Damper body end	-251.3360	-267.5590	308.5060
Outer track rod ball joint	-183.3780	-594.7700	107.9450
Inner track rod ball joint	-183.3780	-296.7990	165.0000
Upper spring pivot point	-251.3360	-267.5590	308.5060
Lower spring pivot point	-270.7390	-553.4880	-47.7240
Wheel spindle point	-255.3050	-620.7600	39.1320
Wheel center point	-255.3050	-645.0330	39.1320

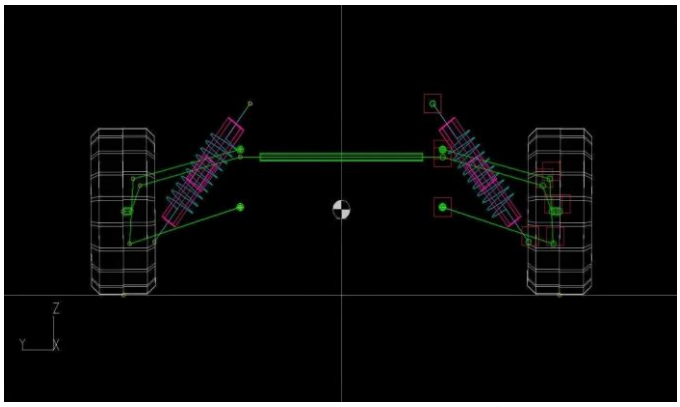

Figure 1: Lotus Shark Suspension Wireframe

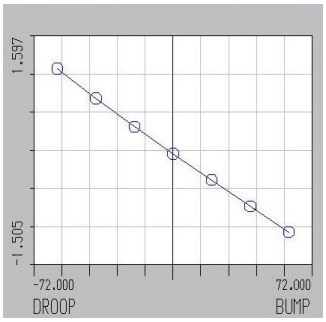

Figure 2: Change in Camber Angle

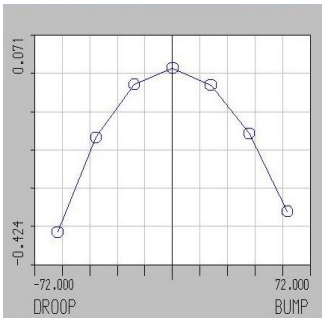

Figure 3: Change in Toe Angle

The first graph represents the change in the camber angle of the front wheels due to suspension droop and bump. According to the graph generated by the Lotus Shark for suspension droop and suspension bump we are getting a change in camber angle by 1.505° and 1.597° respectively which is well within the acceptable range for our design. The second graph represents the change in the toe angle of the front wheels during suspension droop and bump. According to the graph generated by the Lotus Shark for suspension droop and suspension bump we are getting a change in toe angle by 0.424° and 0.071° which is also well within the acceptable range for our design.

IV. STEERING

A linear and predictable steering system is vital to an all-terrain vehicle. The steering of the vehicle is responsible for the control of the lateral motion when the vehicle is in longitudinal motion. A good steering system ensures that the driver should be able to maintain control of the vehicle at all times. The main factors on which the steering system depends are speed of response and driver's input. There are many steering systems each with its advantages and disadvantages. A mechanical steering mechanism with rack and pinion was chosen for our design as this mechanism gives the driver a large range of motion, provides a large degree of feedback and is also very compact. The tie rods used for controlling the wheels were made of high-strength stainless steel AISI 316 with a length of 13.555 inches each, the inner and outer diameter of 7.62 mm respectively. Many objectives were considered during the design of the steering mechanism but the primary objective was to control the lateral motion of the vehicle while the vehicle is in longitudinal motion, to achieve Ackermann geometry, to limit the steering wheel rotation from the lock-to-lock angle, to obtain correct steering angles for each wheel, to achieve slight negative camber in the direction of the turn, and to achieve a small turning radius and steering stability. Another important parameter considered was the distance between the kingpin axis and the mounting hole for the tie rod which along with the ratio of the rack and pinion dictates the overall steering ratio.

International Journal of Engineering Research & Technology (IJERT)
ISSN: 2278-0181
Vol. 10 Issue 04, April-2021

A. Geometry Selection

Traction is an important factor to maneuver a vehicle so we are using Ackermann steering geometry for our design as it provides pure rolling motion or prevents slipping of tires. Whereas Anti-Ackermann geometry is used in high-speed vehicles, which is appropriate for formula one cars. In Ackermann's steering geometry the inner wheel rotates more than the outer wheel.

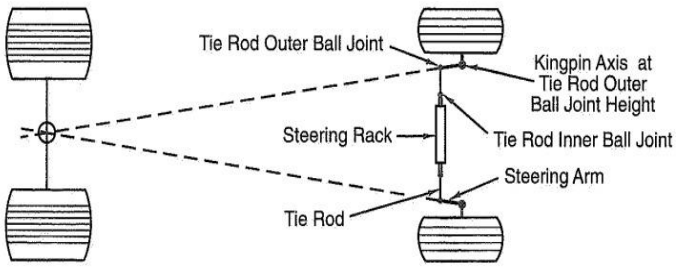

Figure 4: Ackermann Steering Geometry

B. Geometry Setup

1. To achieve perfect Ackermann steering geometry we need to draw an imaginary line inward from the steering pivot points to the point of intersection of the lines drawn between the steering kingpin axis and the center of the rear axle as shown in figure 1.
2. We will draw a line between the pivot points of the wishbone on both sides to determine the rack unit's length.
3. If we draw an imaginary line from the upper and lower wishbone knuckle joints to the points where pivot points of the upper and lower wishbone lie and then extend both the lines until they lie at a common point. Then we will draw another line parallel to these imaginary lines from the steering knuckle joint to the common point of these imaginary lines. Then again, we will draw another line from the common point of the steering knuckle joint line and the pivot point of the wishbone which will give us the length of the tie rod.
4. We took the inner angle of the wheel as 30° for our design (The inner and outer angles must not exceed more than 50°).
5. Then we have calculated the outer angle of the wheel from the inner angle.
6. We took a steering ratio of 8:1 for our design.
7. Then we have calculated lock to lock angle from the steering ratio and inner angle of the wheel.
8. Then we have calculated the number of steering wheel turns.
9. We calculated the Ackermann angle from the inner and outer angles of the wheels.
10. Then we have calculated the turning radius from the wheelbase and Ackermann angle.
11. We took the diameter of the pinion as 28.68 mm.
12. Then we have calculated rack travel from the diameter of pinion and number of steering wheel turns.

C. Steering Calculations

1.) Inner, Outer, and Steering Lock to Lock angle Calculations

$\delta_i = 30°$

$$\mathrm{Cot}\delta_o - \mathrm{Cot}\delta_i = \frac{\text{Track Width}}{\text{Wheelbase}}$$

$$\mathrm{Cot}\delta_o - \mathrm{Cot}\delta_i = \frac{1250.465}{1725.94}$$

$\mathrm{Cot}\delta_o = 0.7245 + 1.73 = 2.4565$

$\delta_o = \mathrm{Cot}^{-1}\, 2.4565 = 22.15$

Steering Ratio = 8: 1

Lock to lock angle = steering ratio $\times \delta_i = 8 \times 30° = 240°$

Number of steering wheel turns $= \frac{240°}{360°} = 0.66$ turns

2. Turning Radius Calculations

Inner angle $(\delta i) = 30°$

Outer angle $(\delta_o) = 22.15°$

Wheelbase $(L) = 1725.94$ mm

R = Turning radius

δ = Ackermann angle

$$\delta = \frac{\delta_i + \delta_o}{2} = \frac{30 + 22.15}{2} = 26.07$$

$26.07° = 0.455$ Radians

$$R = \frac{L}{\delta} = \frac{1725.94}{0.455}$$

R = 3793.274 mm or 12.44 ft

3. Rack Travel Calculations

Diameter of pinion $(D_{pi}) = 28.68$ mm

Number of steering wheel turns $(\eta) = 0.66$

$$\text{Rack Travel} = \frac{\pi \times D_{pi} \times \eta}{2} = \frac{3.14 \times 28.68 \times 0.66}{2} = 29.715 \text{ mm}$$

V. ELECTRIC MOTOR

Different types of motors exhibit different characteristics, which makes it important to evaluate motors on some basic parameters for choosing a particular type of motor for an electric vehicle. Out of all the electric motors available, we are using Brushless DC Motor (BLDC) for our electric dune buggy. Some of the major advantages of BLDC that make them suitable for electric vehicles are having high power density and high power efficiency (95-98 %). It is due to these factors most automotive manufacturers use BLDC motors for their hybrid and electric vehicles.

A. Motor Calculation

1.) Calculation of motor power rating

a) Rolling resistance Calculation

Force due to rolling resistance $(F_{rolling}) = C_{rr} \times m \times g$

Where, Coefficient of rolling resistance $(C_{rr}) = 0.04$

Acceleration due to gravity(g) $= 9.81\ m/s^2$

Mass in kg (m) = 397.8 kg

$F_{rolling} = 0.04 \times 397.8 \times 9.81 = 156.096$ N

b) Gradient resistance Calculation

Force due to gradient resistance $(F_{gradient}) = \pm\, m \times g \times \sin\alpha$

Where, Angle between the ground and slope of the path$(\alpha) = 0°$

Acceleration due to gravity(g) $= 9.81\ m/s^2$

Mass in kg (m) = 397.8 kg

$F_{gradient} = 397.8 \times 9.81 \times \sin 0^{\circ} = 0$ N

c) Aerodynamic drag resistance Calculation

$$F_{\text{aerodynamic drag}} = C_d \times A_f \times \rho \times \frac{v^2}{2}$$

Where, Coefficient of aerodynamic drag $(C_d) = 0.4$

The frontal area of the vehicle $(A_f) = 1.277\ m^2$

Density $(\rho) = 1.2\ kg/m^3$

The velocity of the vehicle in $(v) = 27.77\ m/s$

International Journal of Engineering Research & Technology (IJERT)
ISSN: 2278-0181
Vol. 10 Issue 04, April-2021

$F_{aerodynamic\ drag} = 0.4 \times 1.277 \times 1.2 \times \frac{27.77^2}{2} = 236.34\ N$

d) Total Tractive Force Calculation

$F_{total} = F_{rolling} + F_{gradient} + F_{aerodynamic\ drag}$

Where, F_{total} = Total tractive force

$F_{rolling}$ = Force due to rolling resistance

$F_{gradient}$ = Force due to gradient resistance

$F_{aerodynamic\ drag}$ = Force due to aerodynamic drag resistance

$F_{total} = F_{rolling} + F_{gradient} + F_{aerodynamic\ drag} = 156.096 + 0 + 236.34 = 392.436\ N$

e) Mechanical Power Output Calculation

Power required to overcome the total tractive force (P_{total})

$= F_{total} \times \frac{V}{3600} = 392.436 \times \frac{100}{3600} = 10.901\ kW$

The efficiency of the transmission system (η) = 0.98

Mechanical power output ($M_{tractive}$) $= \frac{P_{total}}{\eta} = \frac{10.901}{0.98} = 11.12\ kW$

2.) Calculation of Motor Speed

$\text{Gear Ratio} = \frac{\text{No. of teeth of Axle Sprocket}}{\text{No. of teeth of Motor Sprocket}} = \frac{35}{20} = 1.75$

$\text{Vehicle Speed} = \frac{R_W \times N}{168 \times \text{Gear Ratio}} = \frac{5.25 \times 3500}{168 \times 1.75} = 62.5\ mil/hr$

Where, R_w = Radius of Wheel

N = Speed of Motor

$\text{Wheel Speed} = \frac{N}{\text{Gear Ratio}} = \frac{3500}{1.75} = 2000\ RPM$

3.) Calculation of Motor Torque

$T = \frac{60}{2 \times \pi} \times \frac{P \times 1000}{n} = \frac{60}{2 \times \pi} \times \frac{11.12 \times 1000}{3500} = 30.35\ Nm$

Where, T = Motor Torque

n = Motor Speed

P = Motor Rating

TABLE VII. Motor Specifications

Rated Power	11.115 kW
Rated Torque	30 Nm
Rated Voltage	72 V
Rated Current	200 A
Power Factor	1
Efficiency	90.2 %

VI. BATTERY

We are using Lithium-ion batteries in our current design because it has high energy efficiency, lack of memory effect, long life cycle, high energy density, and high-power density. These advantages allow them to be smaller and lighter than other conventional rechargeable batteries such as lead-acid batteries, nickel-cadmium batteries, and nickel-metal hydride batteries.

A. Battery Power Calculation

Based on the power rating of Electric Motor, the selection of battery is done.

$P = \frac{E}{(1000 \times t)}$

Where, P = Power in kW

t = Time in hr

E = Energy in Wh

So, $P \times 1000 \times t = E$

Therefore, $E = 11.5 \times 1000 \times 1 = 11500\ Wh$

Battery discharging time at full load

$= \text{Battery rating} \times \frac{\text{Battery Volt}}{\text{Applied load}} = 100 \times \frac{72}{11500} = 0.626\ hr$

TABLE VIII. Battery Specifications

Nominal capacity	100 Ah
Nominal battery voltage	24 V
Continuous charge and discharge current	100 A
Watt-hours	2640 Wh
Charging time	50 minutes

VII. ELECTRONIC SYSTEM

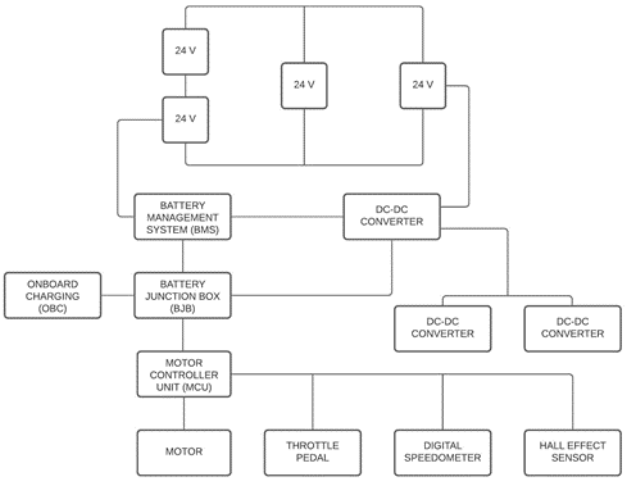

Figure 2: The layout of the Electronic System

Battery: In our current design four Lithium-ion battery packs of 24V each were used. In our design two battery packs were connected in series connection and then these battery packs were connected in parallel connection with the other two battery packs which are also connected in parallel connection.

Battery Management System (BMS): A battery management system is an electronic system that manages a rechargeable battery, such as by protecting the battery from operating outside its safe operating area, monitoring its state, calculating secondary data, reporting that data, controlling its environment and authenticating or balancing it.

International Journal of Engineering Research & Technology (IJERT)
ISSN: 2278-0181
Vol. 10 Issue 04, April-2021

DC-DC Converter: A DC-to-DC converter is an electronic circuit or electromechanical device that converts a source of direct current (DC) from one voltage level to another. It is a type of electric power converter. Power levels range from very low (small batteries) to very high (high-voltage power transmission).

Battery Junction Box (BJB): Battery Junction Box (BJB) is a switching unit for the battery in an electric vehicle. It connects or disconnects the components in the vehicle, which are running on battery power. With one or more bus interfaces, these components are networked with the entire vehicle. The BJB is usually a switching box that switches the high-voltage connection on or off. It ensures that the high voltage is only applied to the necessary contacts when the vehicle is switched on. In these vehicles, the high voltage can be up to 1000 V. It also has a safety function in case of danger, it disconnects the high-voltage battery from the electrical system including all electrical components of the vehicle.

Onboard Battery Charger (OBC): The onboard battery charger is a system built into the vehicle to recharge the high voltage battery from the AC grid while the vehicle is parked.

Motor Controller Unit (MCU): The MCU converts the battery pack's DC power source to an AC power supply to drive the propulsion motor. During vehicle braking, it can regenerate DC power back to the battery pack for charging. The main objective of using an MCU is to control the speed and to start or stop the motor in a more accurate way.

Motor: We are using a Brushless DC Motor (BLDC) of 11.12 kW in our design. The Brushless DC motor is almost similar to a DC motor with permanent magnets and because of the absence of commutator and brush arrangement they are called brushless.

Digital Speedometer: A digital speedometer is a device that displays a digital readout of the instantaneous speed of a vehicle.

Hall Effect Sensor: A Hall effect sensor is an electronic device that is designed to detect the Hall effect, and convert its findings into electronic data, either to switch a circuit on and off, provide a measurement of a varying magnetic field, be processed by an embedded computer or displayed on an interface. Using magnetic fields, Hall effect sensors are used to detect variables such as the proximity, speed, or displacement of a mechanical system.

VIII. BRAKE

We are using a hydraulic disc brake system for the electric dune buggy. The brake has to provide enough force to completely stop the wheel at the end of the acceleration run, it also has to be cost-effective. Hydraulic disc brakes dissipate heat thoroughly and distribute heat more evenly than traditional mechanical brakes, which means that hydraulic brakes are more likely to last longer. This cause is due to brake fluid that resists heat and compression in a hydraulic brake system. The final results increase safety in vehicles with hydraulic disc braking systems. Hydraulic brakes are also one of the most accessible systems to repair due to the readily available disc brake parts. Hydraulic brakes are regarded as sealed off closed systems because they do not lose fluid when functioning correctly. Therefore, you should only see leaks when the brake system is damaged. Disc, calipers, and master cylinders were considered after aftermarket parts were studied for their prices and performances. In our design, we are using floating-type calipers. After considering the above calculation as well as the actual diameter of the front and rear axle of the dune buggy the following dimension of the disc is selected. The dimensions of the cylinder and caliper piston are all selected based on standard market product availability and sizing.

Calculations for Brake

The gross weight of the vehicle (W) $= 307.8 \times 9.81 = 3019.5$ N

Brake line pressure: Area of master cylinder $= 78.53\ mm^2$

Pedal Ratio $= 4:1$

The normal force on pedal $= 350$ N

$$\text{Brake line pressure (BP)} = \frac{(\text{Pedal ratio} \times \text{Force on the pedal})}{\text{Area of the master cylinder}}$$

$$= \frac{4 \times 350}{78.53} = 17.82 \text{ MPa}$$

Clamping force (CF) $=$ BP $\times$ (Area of caliper piston $\times$ 2)

$$CF = 17.82 \times (\frac{3.14}{4}) \times (25.4 \times 10^{-2})^2 \times 2 = 18059 \text{ N}$$

Rotating force (RF) $=$ CF $\times$ No. of caliper piston $\times$ Coefficient of Friction for brake pads $= 18059 \times 2 \times 0.3 = 10835.4$ N

Braking torque $=$ RF $\times$ Effective disc radius

$= 10835.4 \times 0.09 = 975.18$ Nm

$$\text{Braking Force (BF)} = \frac{\text{Braking Torque}}{\text{Tyre Radius}} \times 0.8 = \left(\frac{975.18}{0.23}\right) \times 0.8 = 3391.93 \text{ N}$$

$$\text{Deceleration (a)} = -\frac{BF}{m} = \frac{(-3391.93)}{307.8} = -11.01\ m/s^2$$

Stopping Distance (ds) $v^2 - u^2 = 2 \times a \times ds$

$$ds = \frac{v^2 - u^2}{2 \times a}$$

Where $u = 27.77\ m/s, v = 0$

$$ds = \frac{0^2 - 27.77^2}{2 \times (-11.01)}$$

$$ds = 34.99 \text{ m}$$

TABLE IX. Specification of Brake

Brake disc	190 mm
Master cylinder diameter	10 mm
Caliper piston diameter	25.4
Total weight of brake unit	12 kg

International Journal of Engineering Research & Technology (IJERT)
ISSN: 2278-0181
Vol. 10 Issue 04, April-2021

IX. DESIGN RENDERINGS

X. CONCLUSION

The basic requirement for a dune buggy is to have a high strength-to-weight ratio. In this study, attempts have been made to simplify the dune buggy design in terms of construction and to optimize its strength and durability. A CAD model of the dune buggy was analyzed by the Finite Element Analysis method in Autodesk Fusion 360. The results of simulations performed under different loading conditions showed that this design has demonstrated adequate resistance against deformation in front, back, and side collision tests. All the necessary improvements in the design can be made after identifying its shortcomings. It is not only economical and convenient but it also takes lesser time for analysis. Later on, the optimal design can be fabricated and tested in real-life conditions. The motor selected for our design can achieve the required torque and speed essential for achieving a top speed of 100 km/hr. The chassis, steering knuckle, and suspension are the only components that were designed and the rest all the components used in this design are standard parts available in the market.

XI. REFERENCES

[1] Milliken WF, Milliken DL. Race Car Vehicle Dynamics. Warrendale: SAE International; 1995.
[2] Gillespie TD. Fundamentals of vehicle dynamics. 2nd ed. Warrendale: SAE International; 2021.
[3] Mahapatra P, Arora G, Aggarwal M, Singh S, Manocha R. (2020) Impact behavior analysis of a newly designed go-kart chassis. Indian Journal of Science and Technology. 13(23): 2336-2344. https://doi.org/10.17485/IJST/v1 3i23.502